# $(e,2e)$ and $(e,3-1e)$ studies on double processes of He at large momentum transfer

N. Watanabe,[1,2] Y. Khajuria,[1] M. Takahashi,[1,2,*] Y. Udagawa,[2] P. S. Vinitsky,[3] Yu. V. Popov,[3,†] O. Chuluunbaatar,[4] and K. A. Kouzakov[5]

[1]*Institute for Molecular Science, Okazaki 444-8585, Japan*

[2]*Institute of Multidisciplinary Research for Advanced Materials, Tohoku University, Sendai 980-8577, Japan*

[3]*Nuclear Physics Institute, Moscow State University, Moscow 119992, Russia*

[4]*Joint Institute for Nuclear Research, Dubna 141980, Moscow Region, Russia*

[5]*Physics Department, Moscow State University, Moscow 119992, Russia*

(Received 12 April 2005; published 9 September 2005)

The double processes of He in electron-impact ionization, single ionization with simultaneous excitation and double ionization, have been studied at large momentum transfer using an energy- and momentum-dispersive binary $(e,2e)$ spectrometer. The experiment has been performed at an impact energy of 2080 eV in the symmetric noncoplanar geometry. In this way we have achieved a large momentum transfer of 9 a.u., a value that has never been realized so far for the study on double ionization. The measured $(e,2e)$ and $(e,3-1e)$ cross sections for transitions to the $n=2$ excited state of $He^+$ and to doubly ionized $He^{2+}$ are presented as normalized intensities relative to that to the $n=1$ ground state of $He^+$. The results are compared with first-order plane-wave impulse approximation (PWIA) calculations using various He ground-state wave functions. It is shown that shapes of the momentum-dependent $(e,2e)$ and $(e,3-1e)$ cross sections are well reproduced by the PWIA calculations only when highly correlated wave functions are employed. However, noticeable discrepancies between experiment and theory remain in magnitude for both the double processes, suggesting the importance of higher-order effects under the experimental conditions examined as well as of acquiring more complete knowledge of electron correlation in the target.

DOI: 10.1103/PhysRevA.72.032705 PACS number(s): 34.80.Dp

## I. INTRODUCTION

The use of the $(e,2e)$ method for measurement of electron momentum distribution in matter was first proposed by Smirnov and Neudatchin in 1966 [1] and later by Glassgold and Ialongo [2], followed by the pioneering experiments of Amaldi *et al.* on a thin carbon film [3] and of Weigold *et al.* on Ar [4]. Such attempts have been eventually developed as binary $(e,2e)$ spectroscopy or electron momentum spectroscopy (EMS) with outcome of many years of intensive and extensive studies [[5–10] and references therein]. It is now well documented that the momentum-dependent $(e,2e)$ cross section or momentum profile is directly related to the one-electron momentum density $|\psi(\boldsymbol{p})|^2$ of the ionized orbital, if the measurement is performed under the so-called high-energy Bethe ridge conditions where the collision kinematics most nearly corresponds to collision of two free electrons with the residual ion acting as a spectator [5–11]. The key concept in connecting the $(e,2e)$ cross section with the one-electron momentum density is the first-order plane-wave impulse approximation (PWIA) [5–10], which requires the following: (i) the incoming and outgoing electron energies have to be large enough to describe all the electrons by plane waves, and (ii) large momentum transfer must be achieved so that the momentum and energy transferred to the target are absorbed by the ejected electron, as in x-ray Compton scattering [12].

The double processes of the two-electron system He, single ionization with simultaneous excitation and double ionization that involve both ionization of a target electron and excitation/ionization of a second target electron, are particularly attractive in examining the concept of the PWIA. There are two reasons behind this aspect. First, the system is simple enough to be the subject of accurate calculations. Second, the double processes must be very sensitive to electron correlation in the target initial state because of the absence of electron correlation in the final one-electron ion state. In this sense, for ionization-excitation processes of He the PWIA can directly probe the one-electron momentum densities $|\psi(\boldsymbol{p})|^2$ of excited orbital components of the target ground-state wave function. On the other hand, in the case of double ionization, the PWIA allows us to observe the two-electron momentum density $|\psi(\boldsymbol{p}_1,\boldsymbol{p}_2)|^2$, as originally pointed out by Neudatchin and Smirnov and their co-workers [9,13,14] with the introduction of the $(e,3e)$ method that detects all the three outgoing electrons in coincidence. In spite of the absorbing interest and fundamental importance, however, very few examinations of the PWIA have been made for the double processes of He. The scarcity of such studies can be accounted for by the experimental difficulties that the total cross section becomes smaller rapidly at larger momentum transfer and that the differential cross sections for the double processes are relatively small, only of the order of $10^{-2}$ or less of the primary single-ionization process that leaves the residual $He^+$ ion in the $n=1$ ground state.

The first EMS experiment on ionization excitation of He was made by Cook *et al.* [15] at an impact energy of 1200 eV in the symmetric noncoplanar geometry. They mea-

*Electronic address: masahiko@tagen.tohoku.ac.jp

†Electronic address: popov@srd.sinp.msu.ru

 ©2005 The American Physical Society

sured momentum profiles for the transitions to the $n=2$ and 3 excited states of $He^+$ as normalized intensities relative to that for the $n=1$ ground ion state. Although statistics of the data were not satisfactory, it was concluded that the PWIA reproduces the experiments well, except at high momentum where distorted-wave effects are expected [16]. Momentum-dispersive measurements were made by Smith *et al.* [17] at an impact energy of 800 eV, but unfortunately their $n=1$ and 2 momentum profiles were individually normalized to theory and hence any intensity comparison with theory was not attempted. The most recent study was conducted by Lermer *et al.* [18] at an impact energy of 1200 eV using the momentum- and energy-dispersive techniques. Although the shape of the $n=2$ momentum profile obtained with the momentum-dispersive technique was similar to those of high-accuracy PWIA calculations using the Cann and Thakkar wave function [19] and a 141-term Kinoshita-type wave function [20], the experimental result was found to give about 35% higher intensity than the theoretical predictions. This observation was supported by another measurement using the energy-dispersive technique. As a result, Lermer *et al.* [18] suggested a failure of the PWIA description of the $n=2$ transition, in contrast with the earlier results [15].

As for double-ionization process of He, to our best knowledge no $(e,3e)$ experiment under the high-energy Bethe ridge conditions has been reported. The possibility of probing the two-electron momentum density has been investigated instead under experimental conditions with relatively large or medium momentum transfer (0.62–2.7 a.u.) and low kinetic energies of the two ejected electrons (9–55 eV) by Lahmam-Bennai *et al.* [21] and by Dorn *et al.* [22], as well as by Moore and Coplan and their co-workers on Mg [23,24] and by Lahmam-Bennai *et al.* on Ar [21]. Although the observed $(e,3e)$ cross sections have been found to bear some fingerprints of the two-electron momentum densities of the targets, the experimental conditions employed have made it difficult to give a definitive answer; inadequacy of describing the slow ejected electrons as plane waves and contributions of higher-order effects have prevented quantitative comparisons of the experiments with theoretical two-electron momentum densities [21,23]. Clearly, the extremely small cross section involved presents a serious obstacle to $(e,3e)$ studies under the high-energy Bethe ridge conditions. Recently, a different, experimentally more feasible approach to the two-electron momentum density, the $(e,3-1e)$ method, has been proposed by Popov *et al.* [25], in which the two fast outgoing electrons are detected in the EMS geometry while leaving the slow outgoing electron undetected. Furthermore, based on PWIA calculations with several wave functions, it was shown that though direct extraction of the two-electron momentum density information from the experiment is impossible, the $(e,3-1e)$ method is very sensitive to electron correlation in the target initial state. Such $(e,3-1e)$ experiment has been conducted by Bolognesi *et al.* [26] on He at an impact energy of 580 eV in the coplanar symmetric geometry, achieving a large momentum transfer of 6 a.u. at its maximum. The acute sensitivity of the $(e,3-1e)$ method to electron correlation in the target has been demonstrated somehow, but at the same time they suggested needs of experiments at higher impact energy and of comparisons between experiment and theory on an absolute scale in order to establish the $(e,3-1e)$ method as a powerful tool for studying electron correlation closely.

Under these circumstances, we have made $(e,2e)$ and $(e,3-1e)$ studies on the double processes of He both experimentally and theoretically. In the present paper we report $(e,2e)$ and $(e,3-1e)$ experiments on He using a recently developed multichannel $(e,2e)$ spectrometer [27] that features high sensitivity. An impact energy of 2080 eV was used in the symmetric noncoplanar geometry and we have thus achieved a large momentum transfer of 9 a.u., a value that has never been realized so far for study on double ionization. Assuming that the $(e,2e)$ primary single-ionization transition to the $n=1$ ground ion state can be described by the PWIA, the experimental $n=2$ momentum profile and $(e,3-1e)$ results are placed on an absolute scale. They are compared with PWIA calculations using various wave functions in terms of both shape and intensity. The present work aims at examining the PWIA for the double processes under the kinematics that most closely approaches the high-energy Bethe ridge conditions compared with those achieved in the previous $(e,2e)$ and $(e,3-1e)$ studies [15,17,18,26].

## II. EXPERIMENTAL METHOD

For electron-impact single-ionization and double-ionization processes of He conservation of linear momentum and energy requires

$$\boldsymbol{p}_{\mathrm{He}^+} = \boldsymbol{p}_0 - \boldsymbol{p}_1 - \boldsymbol{p}_2, \tag{1}$$

$$E_{bind} = E_0 - E_1 - E_2 \tag{2}$$

and

$$\boldsymbol{p}_{\mathrm{He}^+} + \boldsymbol{p}_3 = \boldsymbol{p}_0 - \boldsymbol{p}_1 - \boldsymbol{p}_2, \tag{3}$$

$$E_3 = E_0 - E_1 - E_2 - V_{\mathrm{IP}}^{2+}. \tag{4}$$

Here the $\boldsymbol{p}_j$'s and $E_j$'s $(j=0,1,2,3)$ are momenta and kinetic energies of the incident and outgoing electrons, respectively. $\boldsymbol{p}_{\mathrm{He}^+}$ and $\boldsymbol{p}_{\mathrm{He}^{2+}}$ represent recoil momentum of the residual ion $He^+$ and that of $He^{2+}$. $E_{bind}$ and $V_{\mathrm{IP}}^{2+}$ are ionization energy and the double-ionization threshold of He (79 eV). Since the present experiment involves coincident detection of two outgoing electrons, as discussed below, $\boldsymbol{p}_{\mathrm{He}^+}$ and $E_{bind}$ are fully determined for the $(e,2e)$ processes with the aid of Eqs. (1) and (2). In other words, $\boldsymbol{p}_{\mathrm{He}^+}$ dependence of the $(e,2e)$ cross section can be measured for individual ionization transitions. On the other hand, for the $(e,3-1e)$ process the obtainable quantities are $(\boldsymbol{p}_{\mathrm{He}^{2+}}+\boldsymbol{p}_3)$ and $E_3$, and hence $(\boldsymbol{p}_{\mathrm{He}^{2+}}+\boldsymbol{p}_3)$ dependence of the $(e,3-1e)$ cross section can be measured as a function of the undetected slow outgoing electron energy $E_3$. For the sake of simplicity both $\boldsymbol{p}_{\mathrm{He}^+}$ in $(e,2e)$ and $(\boldsymbol{p}_{\mathrm{He}^{2+}}+\boldsymbol{p}_3)$ in $(e,3-1e)$ are called momentum $\boldsymbol{q}$ here, and in the same manner $(e,2e)$ and $(e,3-1e)$ momentum profiles refer $|\boldsymbol{p}_{\mathrm{He}^+}|$-dependent $(e,2e)$ cross section and

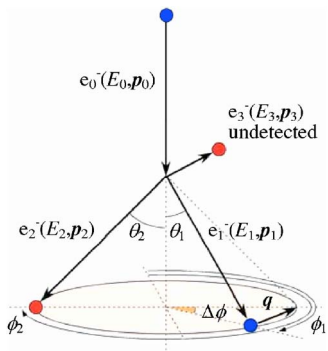


FIG. 1. (Color online) Schematic of the symmetric noncoplanar geometry for study of $(e,2e)$ and $(e,3-1e)$ reactions at large momentum transfer.

$|\boldsymbol{p}_{\mathrm{He}^{2+}}+\boldsymbol{p}_3|$-dependent $(e,3-1e)$ cross section respectively.

Figure 1 shows a schematic diagram of the symmetric noncoplanar geometry that has been widely used for EMS experiments. In this kinematic scheme, two outgoing electrons having equal energies $(E_1=E_2)$ and making equal polar angles $(\theta_1=\theta_2=45°)$ with respect to the incident electron beam axis are detected in coincidence. The magnitude of the momentum $q$ is expressed by

$$q=\sqrt{(p_0-\sqrt{2}p_1)^2+[\sqrt{2}p_1\sin(\Delta\phi/2)]^2} \tag{5}$$

where $\Delta\phi(=\phi_2-\phi_1-\pi)$ is the out-of-plane azimuthal angle difference between the two outgoing electrons detected. If the incident electron energy $E_0$ and momentum $\boldsymbol{p}_0$ are fixed, a given ionization transition $(E_{bind})$ can be selected simply by the choice of detection energy $(E_1=E_2)$ and then $q$ can be determined only by $\Delta\phi$. The same is true for $(e,3-1e)$ experiments, if we detect two fast outgoing electrons with equal energies in the symmetric noncoplanar geometry while leaving one slow outgoing electron undetected.

In the present work an electron-electron-fragment ion triple coincidence spectrometer [27] has been employed to carry out $(e,2e)$ and $(e,3-1e)$ measurements of He simultaneously. Although the spectrometer has been developed for $(e,2e)$ experiments with fixed-in-space molecules, it can be used to produce $(e,2e)$ and $(e,3-1e)$ data by detection of the two fast outgoing electrons only. Details of the spectrometer have been described elsewhere [27], so only a brief summary of the electron detection part needed is given here. An incident electron beam is produced by an electron gun incorporating a tungsten filament. A current of typically 40 $\mu$A is collected on a Faraday cup. Electron impact ionization occurs where the incident electron beam collides with targets from eight nozzles. Scattered electrons leaving the ionization point are limited by a pair of apertures so that a spherical analyzer accepts those with $\theta=45°$ over the azimuthal angle $\phi_1$ and $\phi_2$ ranges from 70° to 110° and from 250° to 290°. In the angular selection a rather large acceptance angle of $\Delta\theta=\pm1.5°$ has been used to achieve higher collection efficiency, though it deteriorates the energy and momentum resolutions obtainable. The electrons passing through the apertures are energy analyzed by the analyzer and then detected by a pair of position-sensitive detectors placed behind an exit aperture. Since a spherical analyzer maintains azimuthal angles for the electrons, both energies and angles can be determined from their arrival positions at the detectors. Thus, by combining a spherical analyzer with a pair of position-sensitive detectors, it is possible to sample the $(e,2e)$ and $(e,3-1e)$ cross sections over a wide range of binding energy ($E_{bind}$ or $E_3+V_{\mathrm{IP}}^{2+}$) and momentum $(q)$ in parallel. This technique significantly improves sensitivity and accuracy of the data compared with the conventional single channel measurements, as drifts in electron beam current and fluctuations in target gas density affect all channels in the same way.

Commercially available He gas (Nippon Sanso, >99.99995%) was used for the $(e,2e)$ and $(e,3-1e)$ measurements. The experiment was performed at an impact energy of 2080 eV, while keeping an ambient sample gas pressure at $2.7\times10^{-4}$ Pa. Two outgoing electrons having about 1000 eV were detected. The instrumental energy and momentum resolutions were 4.3 eV full width at half maximum (FWHM) and about 0.3 a.u. at $\Delta\phi=0°$ for the experiments. No detectable impurities were observed in the binding energy spectra. In this way experimental results have been obtained by accumulation of data for 1 month runtime.

## III. THEORY

There is a considerable body of literature on the PWIA [5–10], so only a brief account will be given here. Within the PWIA the triple differential cross section for an $(e,2e)$ transition of He to an ionic state with a principal quantum number $n$, which is constituted of energetically unresolved sublevels having different orbital angular momentum quantum numbers $l$s, can be written as

$$\frac{d^3\sigma_n}{dE_1d\Omega_1d\Omega_2}=\frac{p_1p_2}{p_0}\sigma_{Mott}\sum_{l=0}^{n-1}(2l+1)|F_{nl}(q)|^2. \tag{6}$$

Here $\sigma_{Mott}$ is the half-off-shell Mott scattering cross section [5] and in the symmetric noncoplanar geometry it is given by

$$\sigma_{Mott}=\frac{1}{4\pi^4}\frac{2\pi\eta}{\exp(2\pi\eta)-1}\frac{1}{K^4}, \tag{7}$$

where $\eta=1/|\boldsymbol{p}_1-\boldsymbol{p}_2|$ and $K$ is the momentum transfer $|\boldsymbol{p}_0-\boldsymbol{p}_1|$. $F_{nl}(q)$ is

$$F_{nl}(q)=(4\pi)^2\int_0^\infty\int_0^\infty r_1^2r_2^2j_l(qr_1)\varphi_{nl}(r_2)\Phi_l(r_1,r_2)dr_1dr_2, \tag{8}$$

where $j_l$ and $\varphi_{nl}$ are the spherical Bessel function and the radial function of a $nl$ orbital for the $\mathrm{He}^+$ ion and $\Phi_l(r_1,r_2)$ is a component of the following expansion of the He ground-state wave function $\Phi(\boldsymbol{r}_1,\boldsymbol{r}_2)$:

$$\Phi(\boldsymbol{r}_1,\boldsymbol{r}_2)=\sum_{l=0}^{\infty}(2l+1)\Phi_l(r_1,r_2)P_l(\cos\theta_{12}) \tag{9}$$

with $P_l$ being the Legendre polynomial. For $(e,3-1e)$ reactions of He, the corresponding fourfold differential cross section is given by [25]

$$\frac{d^4\sigma}{dE_1 dE_3 d\Omega_1 d\Omega_2} = \frac{2}{\pi}\frac{p_1 p_2 p_3}{p_0}\sigma_{Mott}\sum_{l=0}^{\infty}(2l+1)|F_l(q,E_3)|^2, \tag{10}$$

where

$$F_l(q,E_3) = (4\pi)^2\int_0^\infty\int_0^\infty r_1^2 r_2^2 j_l(qr_1)\varphi_l(E_3,r_2)\Phi_l(r_1,r_2)dr_1 dr_2. \tag{11}$$

Here $\varphi_l$ is the partial one-electron state with energy $E_3$ in the Coulomb field of the $He^{2+}$ ion.

In the present study, eight kinds of models for the He ground-state wave function have been examined. The simplest models are the Hylleraas wave function $\Phi_{\mathrm{Hy}}$ [28] and the Hartree-Fock (HF) wave function of Clementi and Roetti $\Phi_{\mathrm{HF}}$ [29]. Both the models are a product of the 1*s* orbital $\phi_{1s}(\boldsymbol{r})$ and hence electron correlation is not taken into account. The Hylleraas wave function is given by

$$\Phi_{Hy}(\boldsymbol{r}_1,\boldsymbol{r}_2) = \phi_{1s}(\boldsymbol{r}_1)\phi_{1s}(\boldsymbol{r}_2) \tag{12}$$

where

$$\phi_{1s}(\boldsymbol{r}) = \sqrt{4\alpha^3}e^{-\alpha r}Y_{0,0}(\hat{\boldsymbol{r}}) \quad \text{with } \alpha = 27/16.$$

Total energies of the Hylleraas and HF wave functions are −2.8477 and −2.8617 hartree, respectively.

The next model is the Hylleraas-Eckart-Chandrasehkar (HEC) wave function with radial correlation [28,30,31], which gives a total energy of −2.8757 hartree.

$$\Phi_{HEC}(\boldsymbol{r}_1,\boldsymbol{r}_2) = \frac{1}{\sqrt{N}}[\exp(-\alpha r_1 - \beta r_2) + \exp(-\alpha r_2 - \beta r_1)], \tag{13}$$

where $N$ is the normalization coefficient and $\alpha$=1.188 530 and $\beta$=2.183 171. To examine effects of both radial and angular correlations on momentum profiles we have used the following three wave functions; a 12-component variation of the Chuluunbaatar, Puzynin, and Vinitsky (CPV) wave function $\Phi_{CPV}$ [32,33], a configuration interaction (CI) wave function $\Phi_{CI}$ of Mitroy *et al.* [34], and the Bonham and Kohl (BK) wave function $\Phi_{BK}$ [35]. The CPV wave function is defined as follows:

$$\Phi_{CPV}(\boldsymbol{r}_1,\boldsymbol{r}_2) = \sum_{i,j,k} c_{i,j,2k}U_i(s)V_j(v)W_{2k}(w), \tag{14}$$

with $s=r_1+r_2$, $v=r_{12}/(r_1+r_2)$, $w=(r_1-r_2)/r_{12}$,

$$U_i(s) = \sqrt{\frac{i!(2\alpha_i)^6}{(i+5)!}}e^{-\alpha_i s}L_i^5(2\alpha_i s),$$

$$V_j(v) = \sqrt{2j+3}P_j^{(0,2)}(2v-1),$$

and

$$W_{2k}(w) = \sqrt{\frac{(k+1)(4k+3)}{2(2k+1)}}P_{2k}^{(1,1)}(w).$$

Here $L_i^5$ is the generalized Laguerre polynomial, $P_j^{(q,t)}$ is the Jacobi polynomial, and $\alpha_i$ is a variational parameter. The CI wave function is given by

$$\Phi_{CI}(\boldsymbol{r}_1,\boldsymbol{r}_2) = \sum_{n=1}^{5}\sum_{l=0}^{n-1} c_{nl}\chi_{nl}(r_1)\chi_{nl}(r_2) \times \sum_{m=-l}^{l}\langle l,m;l,-m|0,0\rangle Y_{l,m}(\hat{\boldsymbol{r}}_1)Y_{l,-m}(\hat{\boldsymbol{r}}_2), \tag{15}$$

where $\langle l,m;l,-m|0,0\rangle$ is the Clebsch-Gordan coefficient and $\chi_{nl}(r)$ is the radial part of the natural orbital. The BK wave function is given by

$$\Phi_{BK}(\boldsymbol{r}_1,\boldsymbol{r}_2) = N[\phi(a,b)(1+Ar_{12}e^{-\lambda r_{12}}) + \phi(c,d)(B+Ce^{-\mu r_{12}}) + D\phi(e,f)] \tag{16}$$

with

$$\phi(a,b) = \exp(-ar_1 - br_2) + \exp(-ar_2 - br_1),$$

where $r_{12}=|\boldsymbol{r}_1-\boldsymbol{r}_2|$. Total energies of these CPV, CI, and BK wave functions are −2.9030, −2.9031, and −2.9035 hartree, respectively.

The last two models are a trial function $\Phi_{AMC0}$ (AMC0) of Ancarani *et al.* [36] and the Pluvinage wave function $\Phi_{Pl}$ [37]:

$$\Phi_{AMC0}(\boldsymbol{r}_1,\boldsymbol{r}_2) = N_{AMC0}e^{-Z(r_1+r_2)}e^{r_{12}/2} \tag{17}$$

and

$$\Phi_{Pl}(\boldsymbol{r}_1,\boldsymbol{r}_2) = N_{Pl}e^{-Z(r_1+r_2)}e^{-ik_{Pl}r_{12}}{}_1F_1\left(1-i\frac{1}{2k_{Pl}},2,2ik_{Pl}r_{12}\right) \tag{18}$$

with $N_{AMC0}$=1.343, $N_{Pl}$=1.535, and $k_{Pl}$=0.410. Total energies of the AMC0 and Pluvinage wave functions are −2.8561 and −2.8788 hartree, respectively.

Theoretical $(e,2e)$ and $(e,3-1e)$ momentum profiles have been generated with the PWIA method using the eight kinds of wave functions described above. Furthermore, to see effects of distortion of the incident and outgoing electron waves, we have calculated $(e,2e)$ momentum profiles with the distorted-wave Born approximation (DWBA) method [38,39] using the CI wave function with the aid of the program supplied from McCarthy [40], and $(e,3-1e)$ momentum profiles with the eikonal-wave impulse approximation (EWIA) [5,41] and the EWIA+SC (semiclassical) [26,42,43] methods using the Hylleraas, HEC, and BK wave functions. [For details about application of the EWIA methods to $(e,3-1e)$ reactions, see Ref. [26].] To make comparisons with the experiments, all the theoretical $(e,2e)$ and $(e,3-1e)$ momentum profiles have been folded with the momentum resolution of the spectrometer according to the procedure of Migdall *et al.* [44].

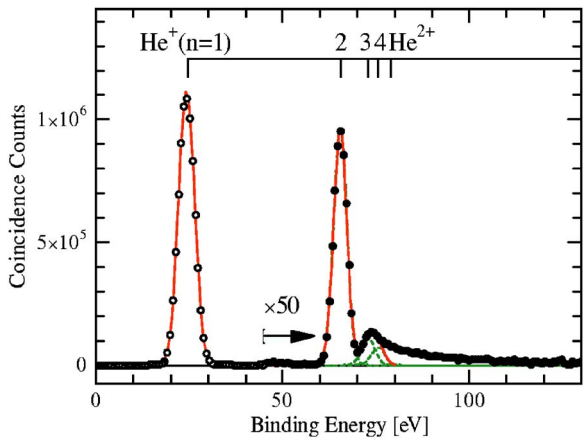


FIG. 2. (Color online) Experimental binding energy spectrum of He obtained at an impact energy of 2080 eV. Note that the spectrum above $E_{bind}$=45 eV is scaled by a factor of 50.

## IV. RESULTS

### A. Binding energy spectrum

In Fig. 2 we show a binding energy spectrum of He obtained at an impact energy of 2080 eV, which was constructed by summing all coincidence signals over the entire $\Delta\phi$ range covered and by plotting the coincidence counts as a function of $E_{bind}(=E_0-E_1-E_2)$. Vertical bars indicate ionization energies [45], showing the transitions to the $n=1$ and 2 states of $He^+$ at $E_{bind}$=24.6 and 65.4 eV and double-ionization continuum at $E_{bind}>V_{IP}^{2+}$. Note that the data responsible for the double processes at $E_{bind}\geqslant 45$ eV are scaled by a factor of 50 for ease of comparison. It is evident that a significant multichannel advantage has been realized and the binding energy spectrum has been obtained with substantially improved statistics compared with those achieved in the previous EMS studies on He [5–10,15,17,18].

Also evident from Fig. 2 is that while the $n=1$ transition is energetically well separated, the instrumental energy resolution does not allow a complete separation of the $n=2$ transition from the adjacent $n=3$ transition. However, it is possible to accurately extract contribution of the $n=2$ transition by deconvolution. In the deconvolution procedure a Gaussian curve with a width of the instrumental energy resolution was assumed for each single-ionization transition. The best fits to the experiment are shown in the figure as broken lines and the solid line is their sum. A similar fitting procedure was repeated for a series of binding energy spectra at each $\Delta\phi$ to produce experimental $(e,2e)$ momentum profiles for the $n=1$ and 2 transitions. They were obtained by plotting the area under the corresponding Gaussian curve as a function of $q$. Similarly, $(e,3-1e)$ momentum profiles at $E_3=10(E_1=E_2=996)$ and $E_3=20$ eV$(E_1=E_2=991$ eV) were generated by plotting all the intensities summed over a binding energy range of 10 eV at $E_{bind}$=84–94 and 94–104 eV as a function of $q$ and by multiplying a factor of 27.2 eV/Hartree/10 eV to convert the intensities to those in atomic units.

### B. $(e,2e)$ and $(e,3-1e)$ momentum profiles

Although the absolute cross section cannot be determined with the present experiment, the relative magnitudes of the individual transitions are maintained. Thus, by normalizing a certain experimental momentum profile to an associated theoretical one, one can place all other experiments on an absolute scale. Normalization of the present experimental data was made as follows. First, we normalized the experimental $n=1$ momentum profile to the associated PWIA calculation using the CI wave function (PWIA/CI) by fitting the area of the experiment up to $q=1.7$ a.u. to that of theory, because it is known that the PWIA provides a very good description of the $n=1$ transition except at high momentum [5–10,15–18]. The results are shown in Fig. 3 where the top and bottom panels represent logarithmic and linear plots of the data, respectively. Then the normalization factor obtained for the $n=1$ transition was subsequently applied to other experimental data, namely the experimental momentum profiles for the $n$

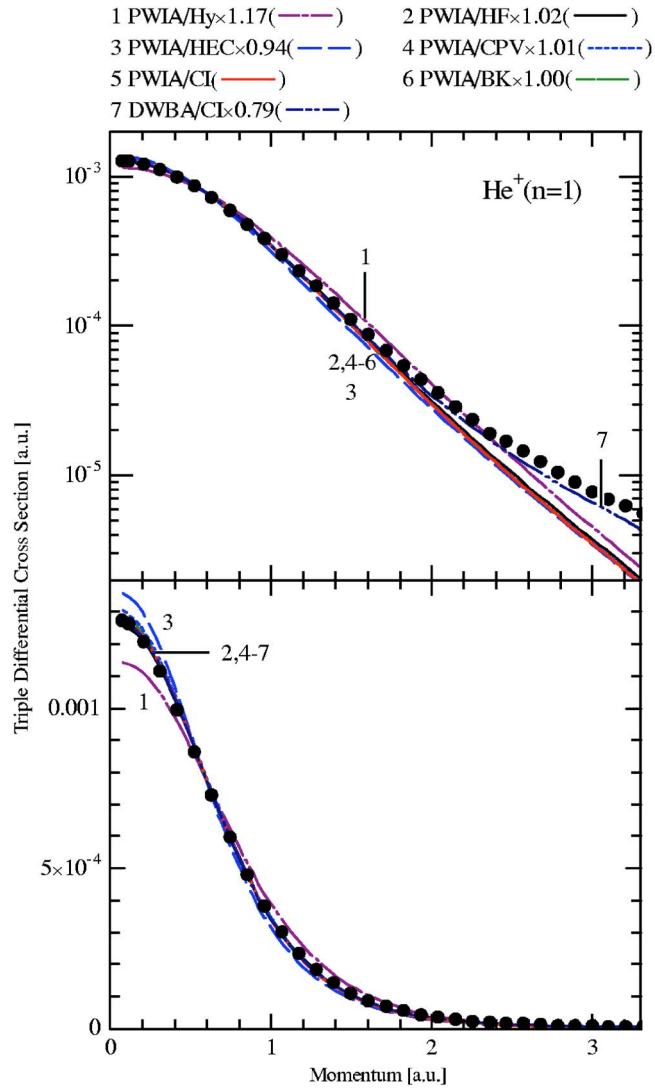


FIG. 3. (Color online) Comparison of experimental $(e,2e)$ momentum profile of He for the transition to the $n=1$ ground ion state with associated theoretical calculations using various variational wave functions. The theoretical momentum profiles are folded with the experimental momentum resolution. All the experimental and theoretical momentum profiles are shown as normalized intensities relative to the PWIA/CI cross section for the $n=1$ ground state of $He^+$. See text for details.

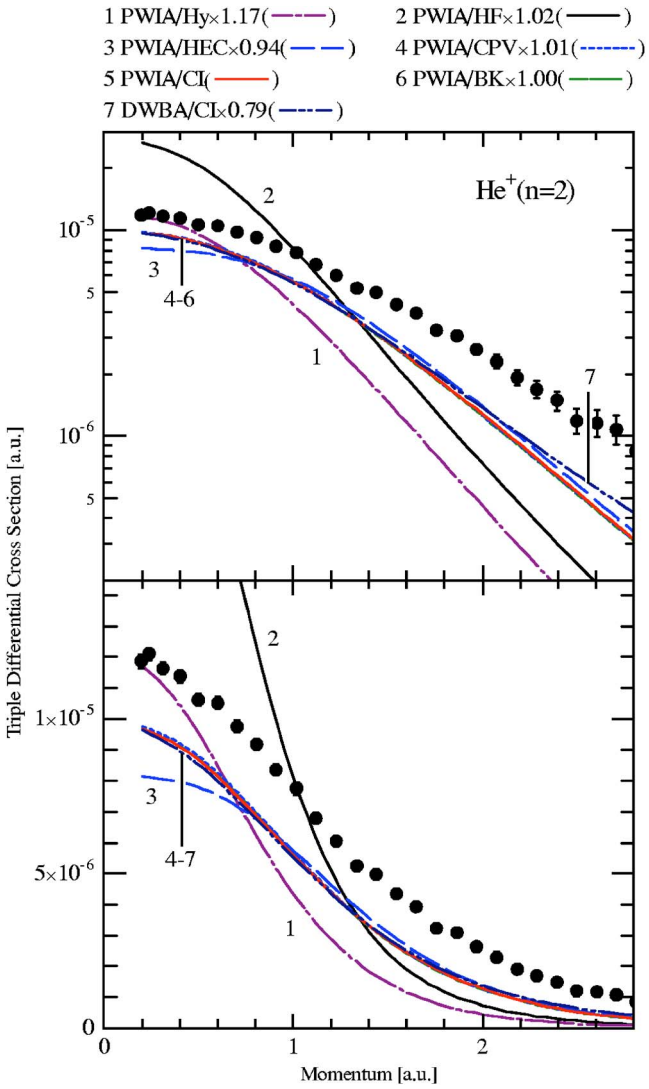


FIG. 4. (Color online) Comparison of experimental $(e,2e)$ momentum profile of He for the transition to the $n=2$ excited ion state with associated theoretical calculations using various variational wave functions. The theoretical momentum profiles are folded with the experimental momentum resolution. All the experimental and theoretical momentum profiles are shown as normalized intensities relative to the PWIA/CI cross section for the $n=1$ ground state of $He^+$. See text for details.

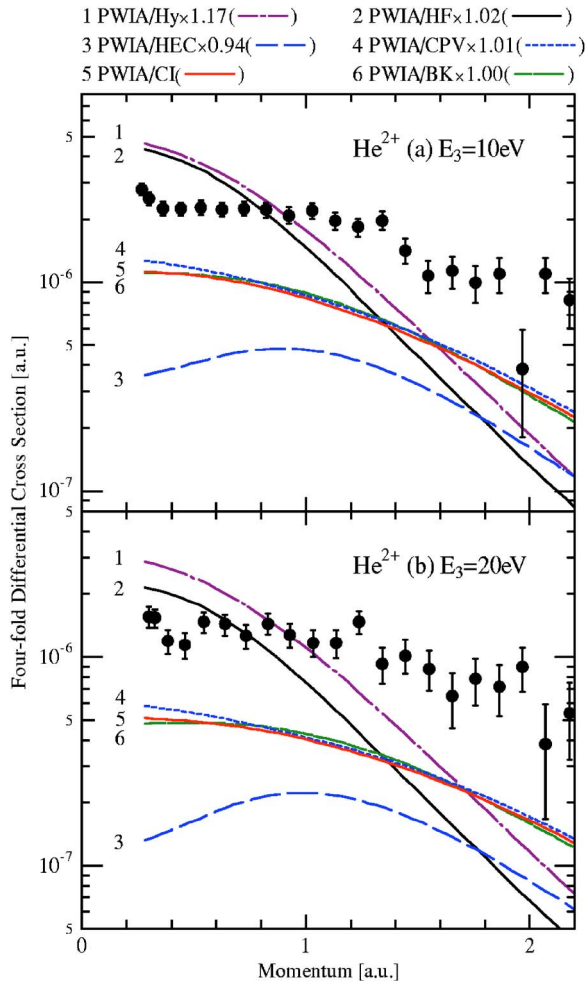


FIG. 5. (Color online) Comparison of experimental $(e,3-1e)$ momentum profiles of He for the doubly ionized $He^{2+}$ with $E_3=$(a) 10 and (b) 20 eV with associated PWIA calculations using various variational wave functions. The theoretical momentum profiles are folded with the experimental momentum resolution. All the experimental and theoretical momentum profiles are shown as normalized intensities relative to the PWIA/CI cross section for the $n=1$ ground state of $He^+$. See text for details.

$=2$ transition and $(e,3-1e)$ processes. Thus all of the experimental and PWIA/CI momentum profiles share an absolute scale throughout the present paper.

Also included in Fig. 3 are theoretical $n=1$ momentum profiles by the PWIA calculations using the Hylleraas, HF, HEC, CPV, and BK wave functions and the DWBA calculation using the CI wave function, which are scaled by factors of 1.17, 1.02, 0.94, 1.01, 1.00, and 0.79, respectively. Each scaling factor has been obtained so that the area of the corresponding theoretical momentum profile up to $q=1.7$ a.u. is the same as that of the PWIA/CI $n=1$ momentum profile.

Figure 4 compares the normalized experimental $n=2$ momentum profile with the associated PWIA/CI and DWBA/CI calculations. Likewise, Figs. 5(a) and 5(b) show the normalized $(e,3-1e)$ momentum profiles at $E_3=10$ and 20 eV, respectively, together with the corresponding PWIA/CI calculations. Also included in Figs. 4 and 5 are the associated PWIA calculations using the Hylleraas, HF, HEC, CPV and BK wavefunctions. All the theoretical momentum profiles in Figs. 4 and 5, except for the PWIA/CI calculations, are scaled by the factors obtained for the $n=1$ transition. This attempt facilitates comparisons of the experiments with various theoretical calculations on a common intensity scale, while they are presented based on the PWIA/CI cross section for the $n=1$ transition. Hence all of the $(e,2e)$ and $(e,3-1e)$ momentum profiles can be regarded as having been placed on an absolute or quasi-absolute scale.

Figures 6 and 7 compare the normalized experimental $(e,2e)$ and $(e,3-1e)$ results with the associated PWIA calculations using the AMC0 and Pluvinage wave functions, which are scaled by a factor of 1.06 and 1.24 respectively in the same spirit as was done in Figs. 3–5. Note that the AMC0 and Pluvinage wave functions exactly satisfy the Kato cusp

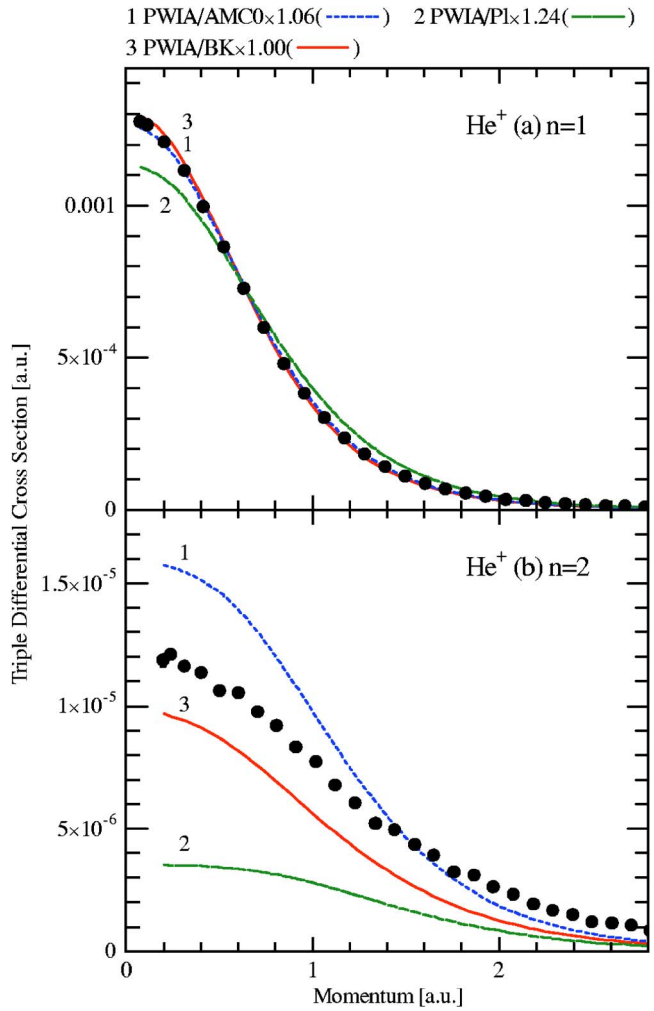


FIG. 6. (Color online) Comparison of experimental $(e,2e)$ momentum profile of He for the transition to (a) the $n=1$ ground ion state and (b) the $n=2$ excited ion state with associated PWIA calculations using the AMC0, Pluvinage, and BK wave functions. The theoretical momentum profiles are folded with the experimental momentum resolution. All the experimental and theoretical momentum profiles are shown as normalized intensities relative to the PWIA/CI cross section for the $n=1$ ground state of $He^+$. See text for details.

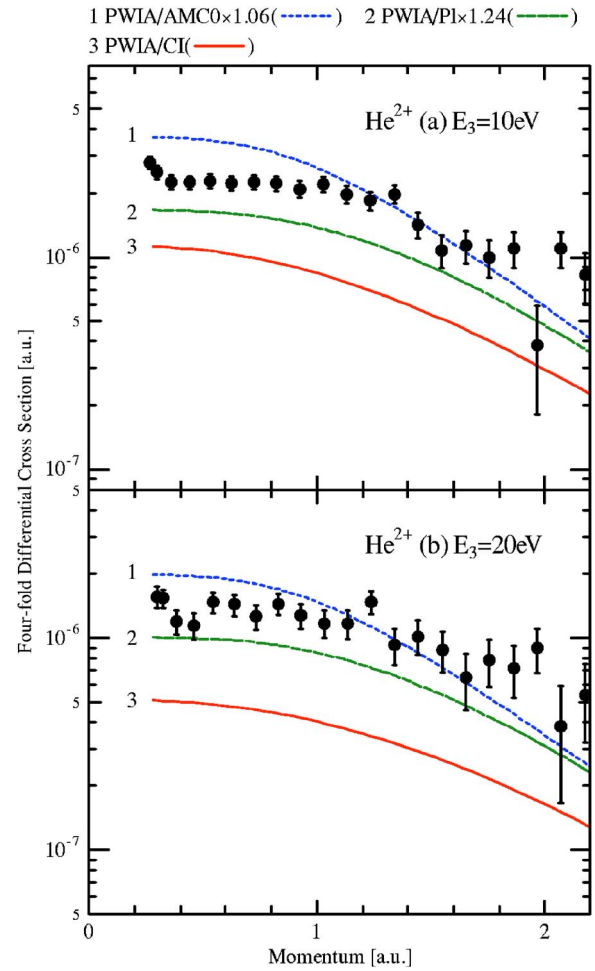


FIG. 7. (Color online) Comparison of experimental $(e,3-1e)$ momentum profiles of He for the doubly ionized $He^{2+}$ with $E_3=$(a) 10 and (b) 20 eV with associated PWIA calculations using the AMC0, Pluvinage, and BK wave functions. The theoretical momentum profiles are folded with the experimental momentum resolution. All the experimental and theoretical momentum profiles are shown as normalized intensities relative to the PWIA/CI cross section for the $n=1$ ground state of $He^+$. See text for details.

conditions [46], though qualities of the two wave functions are rather poor in terms of total energy compared with the highly correlated CPV, CI, and BK functions. For ease of comparison, the PWIA/BK calculations are shown again in Figs. 6 and 7 as a representative of the variational wave functions employed in Figs. 3–5. Such additional attempts with Figs. 6 and 7 are motivated by recent theoretical studies [36,47,48]. In the studies the Pluvinage wave function was used within the first Born approximation and it was found to reproduce well absolute-scale $(e,3e)$ experiments on He at small momentum transfer [49]. However, Ancarani *et al.* [36] have concluded that the observations may be fortuitous based on results of their careful analysis, and suggested that the AMC0 and Pluvinage wave functions should be examined for electron-impact ionization-excitation processes of He to discuss the issue more generally.

## V. DISCUSSION

### A. Single ionization

It is immediately clear from Fig. 3 that all the PWIA calculations are in general agreement with the experimental $n=1$ momentum profile. This is consistent with previous EMS studies that the PWIA provides a very good description of the binary $(e,2e)$ reaction for the $n=1$ transition of He at impact energy above 200 eV [5,10, and references therein]. In particular, the PWIA calculation using the uncorrelated HF wave function is indistinguishable in shape from the calculations using the highly correlated CPV, CI, and BK wave functions, and all of them satisfactorily reproduce the experimental $n=1$ momentum profile, except at high momentum, if the calculation was selected as a standard for the normalization procedure described in Sec. IV B. The minute discrepancy between experiment and PWIA at high momentum is almost completely resolved by the DWBA/CI calculation.

Clearly, in the $n=1$ transition there are no noticeable effects of electron correlation in the target as well as of electron wave distortion except at high momentum.

On the other hand, the experimental $n=2$ momentum profile in Fig. 4 is different from theory and the difference largely depends on the wave function employed. Consider first the PWIA calculations using the uncorrelated Hylleraas and HF wave functions. It is evident that there is a marked difference in shape between the experiment and the two calculations; the PWIA/Hylleraas and PWIA/HF cross sections rapidly decrease with every increase in $q$, unlike the experimental results. This shape difference is greatly reduced by the PWIA calculation using the radially correlated HEC wave function, and further reduced by those using the CPV, CI, and BK wave functions with both radial and angular correlations, showing that the $n=2$ ionization-excitation process is largely influenced by electron correlation effects in the target initial state. Interestingly, the CPV, CI, and BK wave functions with almost the same total energies give the $n=2$ momentum profiles that are indistinguishable from each other, although they have different nature [see Eqs. (14)–(16)]. In spite of the shape agreement, however, a noticeable difference between experiment and PWIA still remains in intensity; the experiment shows about 30% higher intensity than the PWIA/CPV, PWIA/CI, and PWIA/BK predictions, supporting the observation of Lermer *et al.* [18] at an impact energy of 1200 eV.

It is also clear from Fig. 4 that the DWBA/CI calculation is similar to the PWIA/CI, PWIA/BK, and PWIA/CPV calculations, leaving the intensity difference between experiment and PWIA unresolved. Thus it is unlikely that the intensity difference originates mainly in distorted-wave effects. This is supported by the previous theoretical study of McCarthy and Mitroy [16] in which DWIA calculations have been found to affect the ratio of the summed cross section of the $n=2$ transition up to $q\sim 3$ a.u. to that of $n=1$ by only several percent compared with that of their PWIA/CI results.

An insight into the origin of the observed intensity difference can be gained from an EMS study of Takahashi *et al.* [50,51] where the issue in ionization excitation was examined for the isoelectronic system $H_2$. They have performed EMS experiments on $H_2$ at impact energies of 1200, 1600, and 2000 eV and presented the experimental momentum profiles for the transitions to the $2s\sigma_g$ and $2p\sigma_u$ excited state of $H_2^+$ as normalized intensities relative to that for the transition to the $1s\sigma_g$ ground ion state, in the same manner as attempted here. The most striking feature of their results is the shape of the $2p\sigma_u$ momentum profiles; the experiments exhibit gerade symmetry with a maximum of cross section near the momentum origin at every impact energy employed, while the PWIA requests ungerade symmetry with no intensity at $q=0$. Furthermore, the intensities of the normalized experimental $2s\sigma_g$ and $2p\sigma_u$ momentum profiles have been found to depend upon impact energy, indicating that noticeable contributions of higher-order terms are involved in the experiments. To seek for the origin of the observed differences between experiment and theory, they have examined the second-order terms of the plane-wave Born series model and qualitatively identified contributions of the two-step (TS) mechanism [52,53] as the principal source of the observations [50,51].

Actually, contributions of the TS mechanism can give an acceptable and rational explanation for the intensity difference observed here. Note that the $n=2$ state of $He^+$ is constituted by the $2s$ ($^2S_{1/2}$) and $2p$ ($^2P_{1/2}$ and $^2P_{3/2}$) sublevels that correspond to the $2s\sigma_g$, $2p\sigma_u$, and $2p\pi_u$ states of $H_2^+$, whereas the $n=2$ sublevels are not energetically resolved. Basically, the PWIA involves one interaction of the projectile and a target electron, and the theoretical $(e,2e)$ cross section for the $n=2$ transition of He must be calculated by summing the PWIA contributions of the transitions to the $2s$ and $2p$ sublevels according to Eq. (6). In the calculation, the PWIA contribution for the $2s$ transition has been found to be considerably larger than that for the $2p$ transition, and this fact closely reflects that the He ground-state wave function is rich in $s$ character. On the other hand, the TS mechanism involves two successive half collisions with the two $1s$ target electrons; the ionization excitation can occur through the binary knock-out primary ionization process of one $1s$ target electron, followed or preceded by an excitation process of another $1s$ target electron to an excited state due to collision with the incoming or outgoing electrons. The excitation process involved should be dominated by forward scattering under the present experimental conditions where energies of both the incoming and outgoing electrons are very high compared with the energy loss. Hence the symmetry property of the TS contributions is essentially determined by the primary ionization process involved. As a result, the TS contributions would always give momentum profile with gerade symmetry and show little dependence upon the final ion state produced. Furthermore, by analogy with photon impact, the forward-scattering excitation process involved gives much larger contributions for the "optically allowed" transition from the $1s$ state to the $2p$ state than for the "optically forbidden" transition to the $2s$ state. Thus, contributions of the TS mechanism to the experimental $(e,2e)$ cross section would play an important role, for the transition to the $2p$ sublevels of $He^+$ in particular. To the best of our knowledge there are only a few works that have made theoretical calculations incorporating the second-order effects for the $(e,2e)$ ionization-excitation process of He [54–57]. Unfortunately, all the theoretical works were conducted for the very asymmetric ($E_1 \gg E_2$) coplanar kinematics with small momentum transfer and hence direct comparison with the present experiment is impossible. Such calculations would be required to quantitatively understand a role of the TS mechanism in momentum profile for ionization-excitation processes of He at large momentum transfer as well as of $H_2$ [50,51].

### B. Double ionization

It is evident from Fig. 5 that the theoretical $(e,3-1e)$ momentum profiles exhibit considerable dispersion depending on the wave functions employed. We start discussion with PWIA calculations using the uncorrelated Hylleraas and HF wave functions, as in Sec. V A. These PWIA/Hylleraas and PWIA/HF calculations give $(e,3-1e)$ momentum profiles similar in shape to each other but significantly different from the experimental ones at both $E_3=10$ and 20 eV; the

significant difference in shape is reminiscent of that observed for the $n=2$ transition.

The significant difference in shape is reduced by the PWIA calculations using the HEC wave function with radial correlation in both the cases of $E_3=10$ and 20 eV. A similar observation has been made by Bolognesi *et al.* in a 580 eV coplanar symmetric study [26], in which the radially correlated Silverman-Platas-Matsen (SPM) wave function [58], identical to HEC, has been found to better describe the angular distribution of the experimental $(e,3-1e)$ cross section than the Hylleraas function. They have noted also that the absolute cross section predicted by the impulse model with the Hylleraas wave function is four times larger than the one predicted for the SPM or HEC wave function, but in their study the calculations were individually scaled to the relative-scale experimental data and hence any comparison in intensity between experiment and theory was not made. On the other hand, the present experimental and theoretical momentum profiles are placed on the absolute or quasiabsolute scale in the manner described in Sec. IV B. Thus direct comparisons of the theoretical calculations with the experiments are possible not only in shape but also in intensity. It is evident from Fig. 5 that although the PWIA/HEC functions reduce the shape difference observed for PWIA/Hylleraas and PWIA/HF, a noticeable difference still remains; the PWIA/HEC calculations predict the $(e,3-1e)$ momentum profiles with a maximum at $q\sim 1.0$ a.u., while the experiments exhibit a maximum near the momentum origin. Furthermore, a substantial difference in intensity between experiment and PWIA/HEC is revealed; the HEC wave function underestimates the experimental cross sections by a factor of about 5–10.

Both the shape and intensity differences observed for PWIA/HEC are greatly reduced by the PWIA calculations using the CPV, CI, and BK wave functions with radial and angular correlations. It can be seen from Fig. 5 that the PWIA/CPV, PWIA/CI, and PWIA/BK calculations reproduce well the shape of the experimental momentum profiles, approaching the experimental intensities much more closely than PWIA/HEC. At the same time, one can see the same trend as observed for the $n=2$ transition; in spite of their different nature, the CPV, CI, and BK wave functions with almost the same total energies give momentum profiles that are nearly indistinguishable from each other. Thus it is shown that the three variational wave functions give coherent results throughout the present study. Furthermore, if the theoretical $(e,3-1e)$ momentum profiles are scaled by a factor of about 2.4 and 2.9 in the cases of $E_3=10$ and 20 eV, respectively, they equally agree with the experimental momentum profiles within the experimental uncertainties. These observations convincingly demonstrate that the $(e,3-1e)$ method at large momentum transfer is very sensitive to electron correlation in the target initial state.

For a more detailed understanding of $(e,3-1e)$ processes it comes to the critical issue of enquiring further into the origin of the noticeable difference in intensity between experiment and PWIA. To see effects of distortion of the electron waves on the intensity difference, we have calculated $(e,3-1e)$ momentum profiles with the EWIA and (EWIA+SC) methods, as noted earlier. However, the distortion effects have been found to be practically negligible (within a few percent) when we compare the amplitudes of the EWIA and (EWIA+SC) with that of the PWIA, and hence the results of the eikonal-wave impulse approximation calculations are not presented here.

We believe that there are two major sources of the intensity difference in issue. One source is an incomplete description of the target ground-state wave function. Another source is again contributions of the TS mechanism. In double ionization, the TS mechanism involves the binary knock-out primary ionization process of one $1s$ target electron, followed or preceded by an electron-impact ionization process of another $1s$ target electron to a continuum state. In contrast to the excitation process involved in the TS mechanism for ionization excitation, the corresponding ionization process to a continuum state is always "optically allowed." Hence the TS contributions for double-ionization processes may be more appreciable compared with those to $(e,2e)$ ionization-excitation cross section. This is consistent with the findings of comparative studies on the total single $(\sigma^+)$ and double $(\sigma^{2+})$ ionization cross sections of He using various projectiles such as electron, positron, proton, anitiproton, and highly charged ions [59], although the total cross section is dominated by large impact parameter collisions which are in sharp contrast with the present experimental kinematics. It was shown that the ratio of the total single- and double-ionization cross sections $R=\sigma^{2+}/\sigma^+$ changes with the projectile velocity, and that $R$ exhibits a strong dependence upon the charge sign of the projectile. The former feature is a visible proof of noticeable contributions of higher-order effects, and the latter has been successfully ascribed to constructive (destructive) interference for negatively (positively) charged projectiles between the first-order shake-off and the second-order TS amplitudes [59,60]. Furthermore, at the impact energy of 2080 eV employed in the present work the value of total cross section ratio $R$ for electron projectile is about 1.6 times larger than that of the shake-off limit or high-energy limit [61–63]. Thus contributions of the TS mechanism to the $(e,3-1e)$ cross section can be responsible, to a considerable extent, for the intensity difference observed here.

### C. Comparison with theory using the AMC0 and Pluvinage wave functions

Finally, we examine the AMC0 and Pluvinage wave functions, the issue of which is raised by the recent theoretical studies [36,47,48] as described earlier, in the $(e,2e)$ and $(e,3-1e)$ processes at large momentum transfer.

It is evident from Fig. 6(a) that satisfactory agreement with the experimental $(e,2e)$ $n=1$ momentum profile is obtained by the PWIA/AMC0 culation as well as PWIA/BK, and that the PWIA/Pluvinage calculation reproduces the experiment well. However, for the $n=2$ transition disagreement with the experiments is more remarkable for the PWIA/AMC0 and PWIA/Pluvinage momentum profiles than for the PWIA/BK result. The PWIA/AMC0 culation predicts the $(e,2e)$ cross section to decrease rapidly with increase in

$q$, unlike the experimental results; a marked difference from the experiment is obvious in shape. The PWIA/Pluvinage momentum profile significantly underestimates the experimental intensity by a factor of about 3.0, though it is very similar in shape to the experiment.

By contrast, for the $(e,3-1e)$ processes it can be seen from Fig. 7 that the PWIA/AMC0 and PWIA/Pluvinage momentum profiles are closer to the experiments than PWIA/BK at both $E_3=10$ and 20 eV. The PWIA/AMC0 calculations substantially reduce the intensity difference between experiment and PWIA/BK when we compare them in terms of a total $(e,3-1e)$ cross section summed over the $q$ range covered, while some difference in shape from the experiments is remarked. On the other hand, the PWIA/Pluvinage calculations reproduce well the shape of the experiments, resolving the disagreement in intensity between experiment and PWIA/BK to a great extent. These observations may be surprising, because they seem to suggest that the AMC0 and Pluvinage wave functions are superior to the BK function, which gives a considerably more accurate total energy, in ability of predicting $(e,3-1e)$ cross sections on an absolute scale. However, the marked discrepancies between the experiment and the PWIA/AMC0 and PWIA/Pluvinage calculations for the $n=2$ transition prevent us from making any far-reaching conclusions.

The key, principal feature of AMC0 and Pluvinage wave functions consists in satisfying exactly the Kato cusp conditions, as noted earlier. However, the region of configuration space where the cusp dominates is very small and hence the feature must be of minor importance for determining the momentum profiles. It should be noted that the BK and CPV wave functions approximately satisfy the Kato cusp conditions at the point of triple collision. Nevertheless, the PWIA results using the two wave functions are appreciably different from those using the AMC0 and Pluvinage functions except for the case of $(e,2e)$ reaction with $n=1$ transition. Thus the present study suggests that the observed agreement of PWIA/AMC0 and PWIA/Pluvinage calculations with experiment in the $(e,3-1e)$ case is rather a matter of chance (see also Ref. [36]) than appropriateness, indicating the need of acquiring more complete knowledge of electron correlation in the target.

## VI. SUMMARY

We have reported the $(e,2e)$ and $(e,3-1e)$ experiments on the double processes of He at large momentum transfer, together with the PWIA calculations. The measurements were performed at an impact energy of 2080 eV in the symmetric noncoplanar geometry, where a large momentum transfer of 9 a.u. has been realized. The high sensitivity of the experimental setup enabled us to compare the $(e,2e)$ $n=2$ and $(e,3-1e)$ momentum profiles with the PWIA calculations in terms of not only shape but also magnitude, by assuming that the $(e,2e)$ primary ionization transition to the $n=1$ ground ion state is well described by the PWIA. We have demonstrated that the ionization-excitation and the $(e,3-1e)$ processes at large momentum transfer are very sensitive to electron correlation in the target initial state. At the same time, for both the processes noticeable difference in intensity between experiment and theory was found and its origin has been discussed.

The principal source of the intensity difference observed for the processes has been qualitatively attributed to contributions of the TS mechanism, by analogy with the EMS study on the isoelectronic system $H_2$ [50,51]. Moreover, we have suggested needs of acquiring more complete knowledge of electron correlation in the target ground-state wave function in order to approach true nature of the $(e,2e)$ ionization-excitation and $(e,3-1e)$ double-ionization processes more closely. In parallel with these further theoretical developments, similar experiments at higher impact energies would be desired to build up an accumulation of experimental knowledge on the collision dynamics of the double processes at large momentum transfer and to identify the range of the validity of the PWIA where one can obtain detailed target electronic structure information.

## ACKNOWLEDGMENTS

This research was partially supported by the Ministry of Education, Science, Sports and Culture, Grants-in-Aid for Scientific Research (B), No. 13440170 and for Exploratory Research, No. 14654069.

[1] Yu. F. Smirnov and V. G. Neudatchin, JETP Lett. **3**, 192 (1966).
[2] A. E. Glassgold and G. Ialongo, Phys. Rev. **175**, 151 (1968).
[3] U. Amaldi, A. Egiri, R. Marconero, and P. Pizzella, Rev. Sci. Instrum. **40**, 1001 (1969).
[4] E. Weigold, S. T. Hood, and P. J. O. Teubner, Phys. Rev. Lett. **30**, 475 (1973).
[5] I. E. McCarthy and E. Weigold, Phys. Rep., Phys. Lett. **27**, 275 (1976).
[6] C. E. Brion, Int. J. Quantum Chem. **29**, 1397 (1986).
[7] K. T. Leung, in *Theoretical Models of Chemical Bonding*, edited by Z. B. Maksic (Springer-Verlag, Berlin, 1991), Part 3.
[8] M. A. Coplan, J. H. Moore, and J. P. Doering, Rev. Mod. Phys. **66**, 985 (1994).
[9] V. G. Neudatchin, Yu. V. Popov, and Yu. F. Smirnov, Phys. Usp. **42**, 1017 (1999).
[10] E. Weigold and I. E. McCarthy, *Electron Momentum Spectroscopy* (Kluwer Academic/Plenum Publishers, New York, 1999).
[11] A. Lahmam-Bennani, J. Electron Spectrosc. Relat. Phenom. **123**, 365 (2002).
[12] R. A. Bohnam and H. F. Wellenstein, in *Compton Scattering*, edited by B. Williams (McGraw-Hill, New York, 1977).
[13] V. G. Neudatchin, Y. F. Smirnov, A. V. Pavlitchenkov, and V. G. Levin, Phys. Lett. **64A**, 31 (1977).

[14] Y. F. Smirnov, A. V. Pavlitchenkov, V. G. Levin, and V. G. Neudatchin, J. Phys. B **11**, 3587 (1978).
[15] J. P. D. Cook, I. E. McCarthy, A. T. Stelbovics, and E. Weigold, J. Phys. B **17**, 2339 (1984).
[16] I. E. McCarthy and J. Mitroy, Phys. Rev. A **34**, 4426 (1986).
[17] A. D. Smith, M. A. Coplan, D. J. Chornay, J. H. Moore, J. A. Tossell, J. Mrozek, V. H. Smith, Jr., and N. S. Chant, J. Phys. B **19**, 969 (1986).
[18] N. Lermer, B. R. Todd, N. M. Cann, C. E. Brion, Y. Zheng, S. Chakravorty, and E. R. Davidson, Can. J. Phys. **74**, 748 (1996).
[19] N. M. Cann and A. J. Thakkar, Phys. Rev. A **46**, 5397 (1992).
[20] T. Kinoshita, Phys. Rev. **105**, 1490 (1957).
[21] A. Lahmam-Bennani, C. C. Jia, A. Duguet, and L. Avaldi, J. Phys. B **35**, L215 (2002).
[22] A. Dorn, A. Kheifets, C. D. Schröter, B. Najjari, C. Höhr, R. Moshammer, and J. Ullrich, Phys. Rev. A **65**, 032709 (2002).
[23] B. El-Marji, J. P. Doering, J. H. Moore, and M. A. Coplan, Phys. Rev. Lett. **83**, 1574 (1999).
[24] R. W. van Boeyen, N. Watanabe, J. P. Doering, J. H. Moore, and M. A. Coplan, Phys. Rev. Lett. **92**, 223202 (2004).
[25] Yu. V. Popov, C. Dal Cappello, and K. Kuzakov, J. Phys. B **29**, 5901 (1996).
[26] P. Bolognesi, C. C. Jia, L. Avaldi, A. Lahmam-Bennani, K. A. Kouzakov, and Yu. V. Popov, Phys. Rev. A **67**, 034701 (2003).
[27] M. Takahashi, N. Watanabe, Y. Khajuria, K. Nakayama, Y. Udagawa, and J. H. D. Eland, J. Electron Spectrosc. Relat. Phenom. **141**, 83 (2004).
[28] E. A. Hylleraas, Z. Phys. **54**, 347 (1929).
[29] E. Clementi and C. Roetti, At. Data Nucl. Data Tables **14**, 177 (1974).
[30] C. Eckart, Phys. Rev. **36**, 878 (1930).
[31] S. Chandrasekhar, Astrophys. J. **100**, 176 (1944).
[32] O. Chuluunbaatar, I. V. Puzynin, and S. I. Vinitsky, J. Phys. B **34**, L425 (2001).
[33] O. Chuluunbaatar, Yu. V. Popov, and S. I. Vinitsky, JINR Report No. P4-2002-134, Dubna, 2002 (unpublished).
[34] J. Mitroy, I. E. McCarthy, and E. Weigold, J. Phys. B **18**, 4149 (1985).
[35] R. A. Bonham and D. A. Kohl, J. Chem. Phys. **45**, 2471 (1966).
[36] L. U. Ancarani, T. Montagnese, and C. Dal Cappello, Phys. Rev. A **70**, 012711 (2004).
[37] P. Pluvinage, Ann. Phys. **5**, 145 (1950).
[38] S. T. Hood, I. E. McCarthy, P. J. O. Teubner, and E. Weigold, Phys. Rev. A **8**, 2494 (1973).
[39] E. Weigold and I. E. McCarthy, Adv. At. Mol. Phys. **14**, 127 (1978).
[40] I. E. McCarthy, Aust. J. Phys. **48**, 1 (1995).
[41] R. Camilloni, A. Giardini-Guidoni, I. E. McCathy, and G. Stefani, Phys. Rev. A **17**, 1634 (1978).
[42] L. Avaldi, R. Camilloni, Yu. V. Popov, and G. Stefani, Phys. Rev. A **33**, 851 (1986).
[43] J. B. Furness and I. E. McCarthy, J. Phys. B **6**, 2280 (1973).
[44] J. N. Migdall, M. A. Coplan, D. S. Hench, J. H. Moore, J. A. Tossell, V. H. Smith, Jr., and J. W. Liu, Chem. Phys. **57**, 141 (1981).
[45] A. R. Stringanov and R. S. Svenitskii, *Tables of Spectral Lines of Neutral and Ionized Atoms* (Plenum, New York, 1968).
[46] T. Kato, Commun. Pure Appl. Math. **10**, 151 (1957).
[47] S. Jones and D. H. Madison, Phys. Rev. Lett. **91**, 073201 (2003).
[48] S. Jones, J. H. Macek, and D. H. Madison, Phys. Rev. A **70**, 012712 (2004).
[49] A. Lahmam-Bennani, A. Taouli, A. Duguet, L. Avaldi, and J. Berakdar, Phys. Rev. A **59**, 3548 (1999).
[50] M. Takahashi, Y. Khajuria, and Y. Udagawa, Phys. Rev. A **68**, 042710 (2003).
[51] M. Takahashi and Y. Udagawa, J. Phys. Chem. Solids **65**, 2055 (2004).
[52] T. A. Carlson and M. O. Krause, Phys. Rev. **140**, 1057 (1965).
[53] R. J. Tweed, Z. Phys. D: At., Mol. Clusters **23**, 309 (1992).
[54] S. Saxena, K. S. Baliyan, and M. K. Srivastava, J. Phys. B **20**, L611 (1987).
[55] A. Franz and P. L. Altick, J. Phys. B **28**, 4639 (1995).
[56] P. J. Marchalant, C. T. Whelan, and H. R. J. Walters, J. Phys. B **31**, 1141 (1998).
[57] A. S. Kheifets, Phys. Rev. A **69**, 032712 (2004).
[58] J. N. Silverman, O. Platas, and F. A. Matsen, J. Chem. Phys. **32**, 1402 (1960).
[59] J. H. McGuire, N. Berrah, R. J. Bartlett, J. A. R. Samson, J. A. Tanis, C. L. Cocke, and A. S. Schlachter, J. Phys. B **28**, 913 (1995), and references therein.
[60] J. H. McGuire, Phys. Rev. Lett. **49**, 1153 (1982).
[61] B. L. Schramm, A. J. H. Boerboom, and J. Kistemaker, Physica (Utrecht) **32**, 185 (1966).
[62] A. Müller, W. Groh, U. Kneissl, R. Heil, H. Ströher, and E. Salzborn, J. Phys. B **16**, 2039 (1983).
[63] D. Fischer, R. Moshammer, A. Dorn, J. R. Crespo López-Urruita, B. Feuerstein, C. Höhr, C. D. Schröter, S. Hagmann, H. Kollmus, R. Mann, B. Bapat, and J. Ullrich, Phys. Rev. Lett. **90**, 243201 (2003).